

# Zinc- and Cadmium *meso*-Aryl-Isoporphyrins: Non-Aromatic NIR Dyes with Distinct Conformational Features

Çağla Baş<sup>+</sup>,<sup>[a]</sup> Jens Krumsieck<sup>+</sup>,<sup>[a]</sup> William-Dale Möller,<sup>[a]</sup> Dominik Körner,<sup>[a]</sup> and Martin Bröring<sup>\*[a]</sup>

Dedicated to Lechosław Latos-Grażyński on the occasion of his 70th birthday.

**Abstract:** A series of pyrrolyl and dipyrrolyl isoporphyrins carrying different phenyl and thienyl groups is reported. The compounds are obtained by a one-pot approach in the presence of a template reagent. Thienyl derivatives gave better yields, and were the only subclass to form with steric hindrance. The structural analyses carried out on compounds 1 and 14 revealed distinct conformational differences which are likely to result from an intramolecular NH⋯Cl hydrogen bridge of the pyrrolyl subclass. In addition, this hydrogen

bridge strongly favors one of the two possible atropisomers. Hindered rotation of the *meso*-aryl groups is observed only in the cases of methylbenzothieryl derivatives 10 and 15 and leads to the observation of several diastereomers. NIR absorptions up to 923 nm are found throughout. Electrochemical investigations into the 1e<sup>-</sup> and 2e<sup>-</sup> reduced species unravel axial ligand exchange dynamics for the zinc isoporphyrin radical, and the probable formation of a zinc phlorinate.

## Introduction

Isoporphyrins represent a certain tautomeric form of porphyrin in which one of the inner NH protons is shifted to one of the *meso*-C atoms (Figure 1). Such tautomers have been discussed in the literature since 1961 as possible intermediates in chlorin synthesis.<sup>[1]</sup> The formal migration of an N-bonded proton to one of the bridging methine groups leads to the break-up of the macrocyclic conjugation and thus to a marked loss of stability as this bridging carbon atom changes from sp<sup>2</sup> to sp<sup>3</sup> hybridization. The first isoporphyrins were obtained in the 1970s by nucleophilic attack of water or alcohols on electrooxidized zinc-*meso*-arylporphyrins and studied spectroscopically, revealing intense NIR bands between 750 and 900 nm.<sup>[2]</sup> Subsequently, alternative oxidation methods were applied, and a fair number of iron- and zinc-isoporphyrins could be obtained and studied spectroscopically and structurally.<sup>[3]</sup> However, all systems proved to be too sensitive to unravel their chemistry in more detail. Contact with electrophiles leads to the rapid reversion to the starting porphyrins, while ring opening to linear tetrapyr-

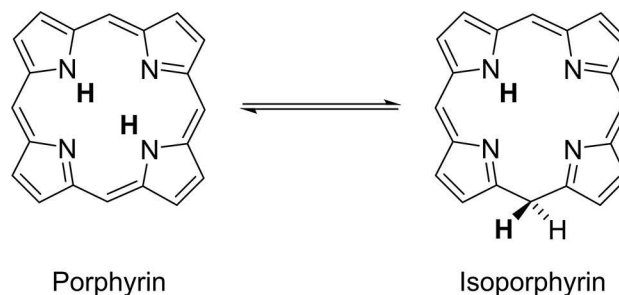


Figure 1. Porphyrin and isoporphyrin as tautomers.

roles of the bilatriene type is reported upon nucleophilic attack. Nevertheless, interest in isoporphyrins of this type has grown significantly in the last years. Recent contributions show such highly reactive isoporphyrins, for example, as reagents for CH activation processes,<sup>[4]</sup> as intermediates in biological cellular respiration<sup>[5]</sup> and as electropolymerized electrode coatings in photovoltaics.<sup>[6]</sup> Related ring-contracted isocorroles with potential in e.g. C–C coupling catalysis serve as important additions to this chemistry.<sup>[7]</sup> A review summarizes the work done in this field before 2015.<sup>[8]</sup>

Isoporphyrins gain additional stability when both hydrogen atoms at the bridging sp<sup>3</sup> carbon atom are substituted by organic residues. This structural motif was first realized ring-synthetically by Smith et al., who received and studied *meso*-dimethyl species like I (Figure 2).<sup>[9]</sup> Recently, we reported a simpler synthetic pathway to stabilized isoporphyrins II by a one-pot approach.<sup>[10]</sup> This type of isoporphyrin formation was serendipitously unraveled during a study of a variation of the Adler-Longo porphyrin synthesis,<sup>[11]</sup> using the Gryko conditions for corrole formation<sup>[12]</sup> and zinc- or cadmium acetate as

[a] Ç. Baş,<sup>+</sup> J. Krumsieck,<sup>+</sup> W.-D. Möller, D. Körner, Prof. Dr. M. Bröring  
Institute of Inorganic and Analytical Chemistry  
TU Braunschweig  
Hagenring 30, 38106 Braunschweig (Germany)  
E-mail: m.broering@tu-bs.de

[\*] These authors contributed equally to this work.

Supporting information for this article is available on the WWW under <https://doi.org/10.1002/chem.202100686>

© 2021 The Authors. Chemistry - A European Journal published by Wiley-VCH GmbH. This is an open access article under the terms of the Creative Commons Attribution Non-Commercial NoDerivs License, which permits use and distribution in any medium, provided the original work is properly cited, the use is non-commercial and no modifications or adaptations are made.

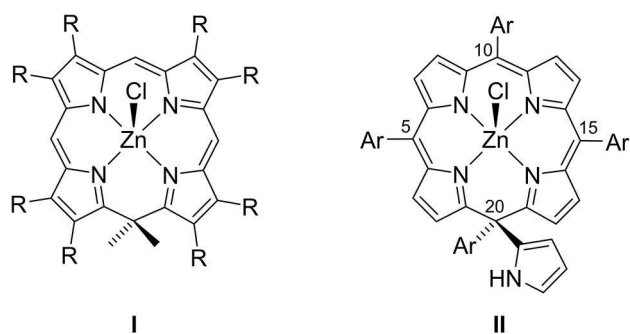


**Figure 2.** Stabilized zinc isoporphyrins I and II, with numbering system for the *meso* positions.

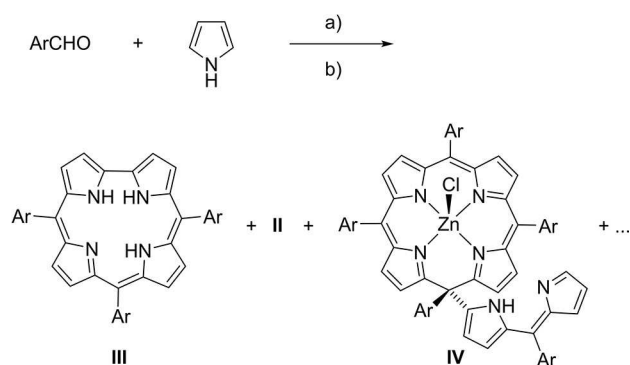
additional template reagents. In some cases, the isoporphyrins emerged even as major products, despite the known sensitivity of this substance class. The isolation of the first derivatives was achieved with relatively little effort by chromatographic separation and crystallization. Investigations into the properties of the new isoporphyrins revealed the characteristic NIR bands known for this macrocycle. Furthermore, first chemical transformations (metal and ligand exchange reactions, borylation at the periphery) proved to be successful and created interest into this compound class for further exploration.

In order to expand the chemistry of isoporphyrins further, we first investigated the general accessibility by the one-pot process in more detail. Here, we focus on the use of differently substituted aryl aldehydes and template metals as starting materials, and on isolation conditions for the obtained porphyrinoids. Furthermore, we were keen to observe the influence of different substituents on stability, structural and spectroscopic characteristics of isoporphyrins for the first time. In this paper, we summarize our results on the preparation and investigation of 15 new isoporphyrin derivatives.

## Results and Discussion

The isoporphyrin one-pot synthesis is carried out in two consecutive steps. In the first step, pyrrole and an aryl aldehyde are condensed under Bronsted acidic conditions to form a mixture of linear oligopyrroles. Shortly after addition of the acid, a clouding of the solution can be observed. Here, increasingly insoluble oligopyrroles precipitate from the equilibrium mixture. The heterogeneous reaction procedure requires very intensive mixing to achieve reproducible yields. In the second step, the nonpolar components of the reaction mixture are extracted and mixed with *p*-chloranil and a template reagent. This treatment leads to ring closure (Scheme 1).

After work-up, the isolated products are the pentapyrrolic metal isoporphyrin II, the tetrapyrrolic free base corrole III and, in some cases, a hexapyrrolic metal isoporphyrin IV. The observation of varying, but generally very small amounts of porphyrin is probably due to the slow decomposition of previously formed isoporphyrins. Products composed of less than four or more than six pyrrole units probably also form<sup>[11b,13]</sup>

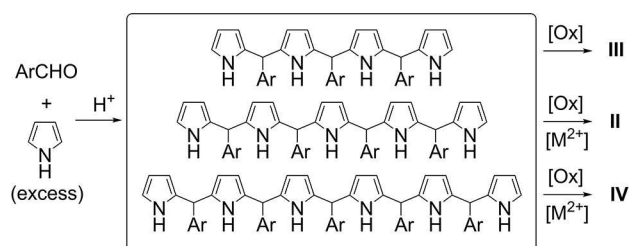


**Scheme 1.** General reaction scheme for the two-step, one-pot preparation, with the observed major products II, III, and IV. a) HCl (aq.), MeOH; r.t., 180 min. b) Zn(OAc)<sub>2</sub> × 2 H<sub>2</sub>O, *p*-chloranil, CHCl<sub>3</sub>, reflux, 60 min.

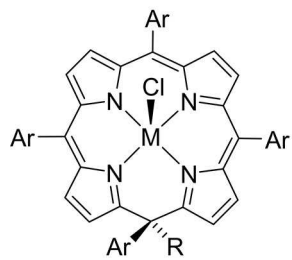
but could not be isolated. Moreover, in the absence of template substances, no isoporphyrins can be detected. These observations lead to the proposed reaction process outlined in Scheme 2.

A number of different aryl aldehydes has been investigated for their eligibility to form new isoporphyrins following the general conditions described above. The successful reactions are summarized in Figure 3. Several other aryl aldehydes failed to produce isoporphyrin products. All heteroaromatic aldehydes except those from thiophene derivatives did not yield any detectable isoporphyrin product. The same observation was made using the sterically hindered 2,6-dichlorobenzaldehyde and mesitylaldehyde. Only traces of the desired macrocycles were obtained from the electron poor aldehydes C<sub>6</sub>F<sub>5</sub>CHO and 4-NO<sub>2</sub>-C<sub>6</sub>H<sub>4</sub>CHO, and isolation of those products was not successful in our hands. 4-F-, 4-CF<sub>3</sub>- and 3,5-di(CF<sub>3</sub>)-benzaldehyde, however, gave fair yields of zinc *meso*-pyrrolyl isoporphyrins II, as did the electron-rich 4-EtO- and 4-Me-benzaldehydes, and benzaldehyde itself. The observed yields are generally in between 4% and 13%. The C<sub>6</sub>H<sub>5</sub>- and the 4-MeOC<sub>6</sub>H<sub>4</sub>-derivatives 1 and 16<sup>[10]</sup> gave somewhat higher yields of 16% and 18%, respectively.

Thienyl aldehyde behaves conspicuously in a positive sense. With this precursor, the isoporphyrin 8 is obtained in a yield of 36%. In addition, the result for the methylbenzothienyl derivative 10 shows that product formation still occurs in significant amounts for thiophenes even with increased steric



**Scheme 2.** Proposal for metal isoporphyrin II/IV and free base corrole III formation by the one-pot strategy.



	<i>R</i>	<i>M</i>	<i>Ar</i>
1	py	Zn	C <sub>6</sub> H <sub>5</sub> (16%)
2	py	Zn	4-MeC <sub>6</sub> H <sub>4</sub> (8%)
3	py	Zn	4-EtOC <sub>6</sub> H <sub>4</sub> (4%)
4	py	Zn	4-FC <sub>6</sub> H <sub>4</sub> (10%)
5	py	Zn	4-CF <sub>3</sub> C <sub>6</sub> H <sub>4</sub> (11%)
6	py	Zn	3,5-(CF <sub>3</sub> ) <sub>2</sub> C <sub>6</sub> H <sub>3</sub> (13%)
7	py	Zn	3,5-(CH <sub>3</sub> ) <sub>2</sub> -4-MeOC <sub>6</sub> H <sub>2</sub> (12%)
8	py	Zn	2-thienyl (36%)
9	py	Zn	2-(5-phenylthienyl) (10%) <sup>[a]</sup>
10	py	Zn	5-(4-methylbenzothieryl) (9%) <sup>[a]</sup>
11	py	Cd	C <sub>6</sub> H <sub>5</sub> (11%)
12	dipy	Zn	C <sub>6</sub> H <sub>5</sub> (14%)
13	dipy	Zn	4-MeC <sub>6</sub> H <sub>5</sub> (5%)
14	dipy	Zn	4-FC <sub>6</sub> H <sub>5</sub> (2%)
15	dipy	Zn	5-(4-methylbenzothieryl) (2%) <sup>[a]</sup>
16	py	Zn	4-MeOC <sub>6</sub> H <sub>4</sub> (18%)
17	dipy	Zn	4-MeOC <sub>6</sub> H <sub>4</sub> (11%)

**Figure 3.** New metal isoporphyrins 1–15, and known zinc 4-methoxyphenyl derivatives 16, 17 (yields in parenthesis). [a] A 3:1 mixture of methanol/water was necessary in the condensation step to observe isoporphyrin formation.

hindrance. A DFT analysis shows that the structures of the phenyl and thienyl substituted zinc isoporphyrins 1 and 8 differ significantly with regard to the dislocation of the perimeter atoms from an average macrocycle plane (Figure 4). The reason for this is probably the smaller size of the thienyl moiety. This allows for enhanced coplanarity of the substituent  $\pi$  system with the macrocyclic one in the thienyl case (calculated rotation between mean squares planes of 53.99° (C5), 45.94° (C10) and 50.39° (C15) for 8, versus 64.24°, 61.77° and 59.74°, respectively, for 1), and thus an energetically favorable enhanced conjugation. As a consequence, the molecule accepts a stronger repulsion of the thiophene H atoms with the  $\beta$ -H atoms of the neighboring C<sub>5</sub>N rings, which gives rise to the observed

increase in saddling distortion.<sup>[14]</sup> Such an intermolecular interaction should push the pyrrole subunits of a linear precursor out of coplanarity and enforce a helical arrangement, which is assumed to be advantageous for zinc binding<sup>[15]</sup> and for the ring closure step.

The condensation and the ring closure steps were further investigated on selected derivatives with Ar=C<sub>6</sub>H<sub>5</sub> 1/12 and Ar=4-MeO-C<sub>6</sub>H<sub>4</sub> 16/17. Since the accumulation of the desired penta- and hexapyrroles in the precipitated material depends on their solubility in the medium and thus presumably on its polarity, the methanol/water ratio was systematically varied. The change in the product composition could be followed after the subsequent oxidation by means of UV/Vis spectroscopy. The intensity of the bands at 360 nm, 420 nm and 640 nm changed with solvent composition, indicating the formation of corrole III and other unknown by-products (Figure 5). The amount of formed isoporphyrins II and IV, however, could not be reliably quantified due to the relatively low extinction coefficients of the Q bands, and to the strong overlap of the major signals at around 450 nm with other absorption bands from the mixture. A complete chromatographic work-up and isolation of the isoporphyrins therefore becomes necessary for each measured point. As it turned out for the observed cases, larger amounts of isoporphyrins were found to be accompanied by medium to low intensities of the bands at 640 nm, which correlates with methanol/water mixtures ranging from 1:1 to 3:1. The optimum composition of the condensation medium for the pentapyrrolic derivative II was found at a methanol/water ratio of 1:1 in both cases 1 (16% + 14% 12) and 16 (18% + 11% 17), while a 3:1 mixture leads to a favored formation of the hexapyrrolic derivatives 12 (12% + 4% 1) and 17 (11% + 3% 16). The amount of HCl added, on the other hand, shows

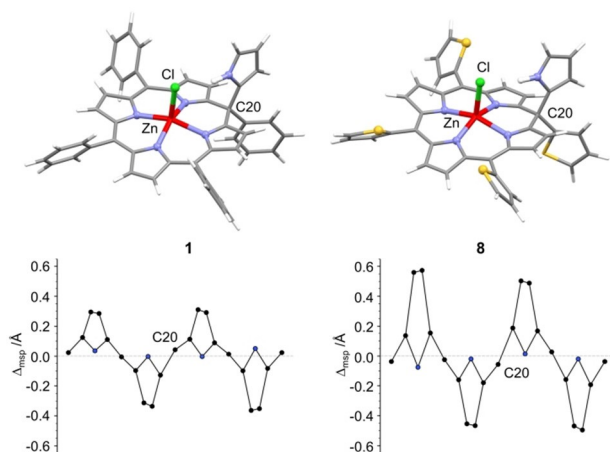


**Figure 4.** Optimized molecular structures of zinc isoporphyrins 1 and 8 (CAM-B3LYP/def2-TZVP/CPCM(CH<sub>2</sub>Cl<sub>2</sub>)), with linear displays of atomic displacements from the mean-squares C<sub>20</sub>N<sub>4</sub> plane.

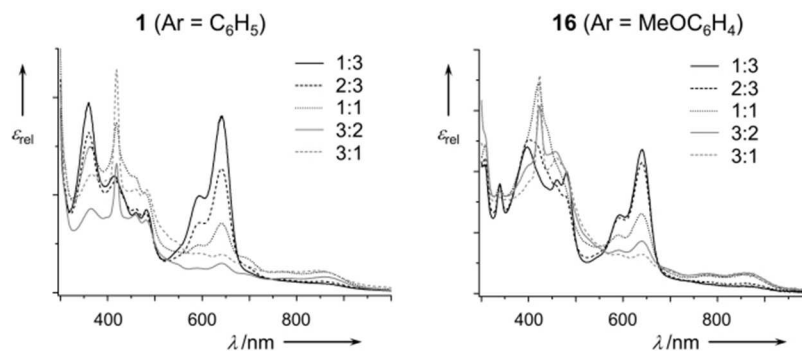


**Figure 5.** Qualitative UV/Vis spectra of reaction product mixtures for **1/12** (Ar=C<sub>6</sub>H<sub>5</sub>, left) and **16/17** (Ar=4-MeOC<sub>6</sub>H<sub>4</sub>, right) using different methanol/water mixtures as solvent in the condensation step.

hardly any influence on the reaction process above a critical minimum amount.

When investigating the ring closure reaction, the focus was laid on the nature of the template reagent. Zinc acetate already used in the preliminary work was found to be the best choice. Cadmium acetate also led to isoporphyrin formation in one case (**11**), but with somewhat lower yields. Acetate salts of the redox-active 3d transition metal ions of manganese, iron, cobalt, nickel and copper, on the other hand, did not yield isolable isoporphyrin products. Interestingly, isoporphyrin could also not be found with zinc chloride as the template reagent. This indicates a complex templating process in which the acetate ions take on supporting tasks in addition to the zinc ions, and in which a redox interference of the metal ion with the oxidative ring closure reaction results in failure.

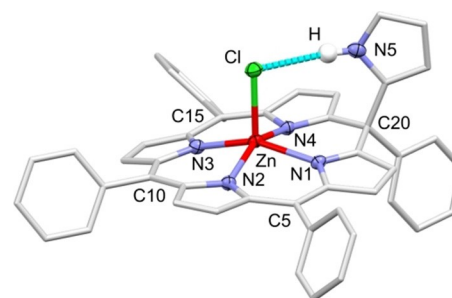
In addition to the reaction procedure, the chromatographic work-up is crucial for the successful preparation of isoporphyrins. In a typical example the solvent is removed, the product mixture is applied to silica and the corrole, which is omnipresent as a by-product, is washed from the column with dichloromethane as the sole eluent. Then, by adding small amounts of ethyl acetate, the more polar isoporphyrins can be eluted. In cases where only traces of the *meso*-dipyrrolyl isoporphyrin **IV** are formed, the *meso*-pyrrolyl derivative **II** is thus obtained in sufficient purity after crystallization from dichloromethane/*n*-hexane. However, if dipyrrolyl isoporphyrin **IV** is present in significant amounts, isolation requires several tedious chromatographic steps, sometimes with high losses. For this reason it can be advantageous to optimize not for maximum yield on total isoporphyrins but rather for minimal occurrence of either the pentapyrrolic form **II** or the hexapyrrolic dipyrrolyl isoporphyrin **IV**.

From the above investigations, it appears that the conditions mentioned in the preliminary study<sup>[10]</sup> are already very well adapted to the preferential formation of isoporphyrins from typical benzaldehydes. Further optimization for different aryl aldehydes may be achieved mainly by varying the solvent polarity in the condensation step (e.g. for **9**, **10** and **15**), and by limiting the formation of the undesired pyrrolyl or dipyrrolyl derivatives through the same measure. However, as the isolation of the products is still tedious and necessary for every

optimization attempt, such efforts will require improved chromatographic methods in each case.

The molecular structures of one pyrrolyl and one dipyrrolyl isoporphyrin **1** and **14** could be determined by single crystal X-ray diffraction. Both compounds crystallize as solvates from dichloromethane/*n*-hexane by vapor diffusion at 4 °C in the monoclinic system with *Z*=4, space group *P*<sub>2</sub><sub>1</sub>/*c* (**1**) and *P*<sub>2</sub><sub>1</sub>/*n* (**14**), respectively. The solvent molecules could only be partially described in both cases. The residual electron density has therefore been removed using the SQUEEZE command in PLATON. Selected molecular parameters for **1** and **14** are compared with the earlier reported data for **16**<sup>[10]</sup> in Table 1. Figures 6 and 7 provide perspective views of the molecular structures.

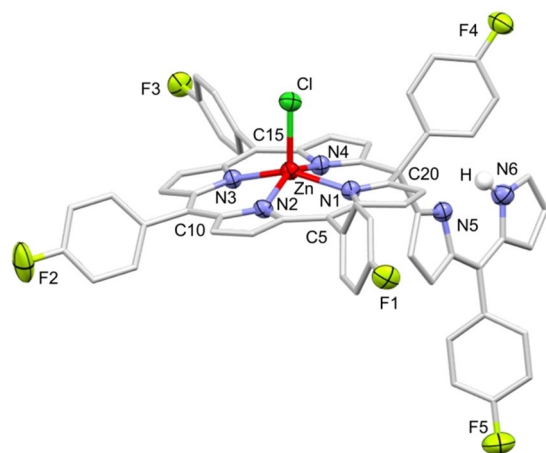
The parameters of the coordination sphere of the zinc atom are very similar in all cases. Thus, all three structures show Zn–N bond lengths between 2.078 Å and 2.139 Å, and the Zn–Cl bond length is always detected between 2.281 Å and 2.324 Å. The displacement of the zinc atom from the mean N<sub>4</sub> plane is also found in a narrow range between 0.475 Å and 0.509 Å. The data from the DFT calculations on **1** and on the thienyl derivative **8** (Zn–N between 2.084 Å and 2.129 Å, Zn–Cl 2.348 Å and 2.342 Å, displacement 0.449 Å and 0.460 Å) reproduce the experimentally determined quantities very well, with the zinc displacement being slightly underestimated and the Zn–Cl bond length slightly overestimated. In zinc isoporphyrin structures with water or methanol as the axial ligand, a



**Figure 6.** Molecular structure of **1**. Thermal ellipsoids are set at 50% probability. Most hydrogen atoms are removed for clarity.

**Table 1.** Selected bond lengths /Å and angles /° from the molecular structures of **1**, **16**<sup>[10]</sup> and **14**.

Compound	<b>1</b> (Ph/py)	<b>16</b> (MeO/py)	<b>14</b> (F/dipy)
Zn–N1	2.130(3)	2.129(3)	2.139(2)
Zn–N2	2.078(3)	2.081(3)	2.088(2)
Zn–N3	2.102(3)	2.101(3)	2.103(2)
Zn–N4	2.124(2)	2.125(3)	2.122(2)
Zn–Cl	2.303(1)	2.324(1)	2.281(1)
N <sub>4</sub> ···Zn/Å <sup>[a]</sup>	0.475	0.477	0.509
Cl···H	2.488	2.649	–
Cl···N <sub>pyrrolyl</sub>	3.330	3.331	–
C20–C1	1.512(4)	1.499(5)	1.513(3)
C20–C19	1.513(4)	1.510(5)	1.511(3)
C20–C <sub>aryl</sub>	1.550(4)	1.545(5)	1.544(4)
C20–C <sub>pyrrolyl</sub>	1.526(4)	1.531(5)	1.528(4)
C1–C20–C19	117.9(3)	118.3(3)	117.7(2)

[a] Displacement of the Zn atom from the N<sub>4</sub> mean squares plane.**Figure 7.** Molecular structure of **14**. Thermal ellipsoids are set at 50% probability. Most hydrogen atoms are removed for clarity.

significantly lower value for the zinc displacement of about 0.31 Å is reported.<sup>[3q,9c]</sup> Thus, the displacement seems to be mainly dependent on the type of axial ligand.

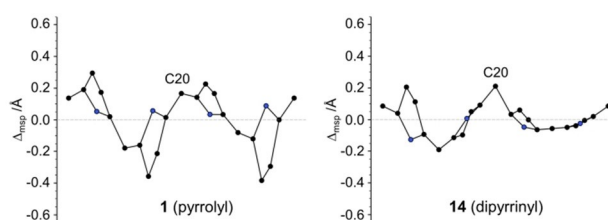
Between the axial chloro ligand and the pyrrolyl substituent in the structures of **1** and **16**, a hydrogen bond with Cl···H distances of 2.488 Å and 2.649 Å is present. Apparently, the isomer in which this H-bridge can be formed on the upper side of the macrocycle is preferred over the isomer with the pyrrolyl residue on the lower side. In the case of **14**, on the other hand, the dipyrrolyl residue is found on the lower side of the isoporphyrin, although no energetic advantage appears obvious from this arrangement. Hydrogen bonding is omitted in this case for steric reasons.

For the bond lengths and angles at the C(sp<sup>3</sup>) position C20, very similar and typical values for a quaternary C atom are found in the experiment and in the calculation. The angles C19–C20–C1 range from 117.7° to 118.3° (calculated for **1**: 117.9°) and are markedly smaller than those at the sp<sup>2</sup>-configured *meso* positions. The other angles at C20 are found between 104.2° and 115.4° (calculated for **1** between 103.0° and 115.2°) and indicate a slight tetragonal distortion of the tetrahedron. A possible differentiation between the pyrrolyl-

and the dipyrrolyl-substituted compound at this position is not apparent.

The macrocyclic conformations of the isoporphyrins **1**, **14** and **16** were analyzed in detail using the porphyrin NSD online tool.<sup>[16]</sup> Figure 8 presents the linear displays of the new compounds **1** and **14**. The relative extents of the major distortion modes doming, ruffling and saddling are summarized in Table 2.

The saddling mode clearly stands out as the main mode for the pyrrolyl derivatives **1** and **16**, while it only plays a minor role for the dipyrrolyl derivative **14**. Here again, the extent of the saddling distortion correlates with the rotation of the aryl substituents (mean value for **1**: 53.77°; for **16**: 58.77°; for **14**: 70.63°): the smaller the rotation from a coplanar arrangement with the C<sub>20</sub>N<sub>4</sub> macrocycle, the stronger is the saddling. Since only the hydrogen bridge between the pyrrolyl substituents and the axial chloro ligands in **1** and **16** exerts a direct influence of the peripheral substituents on the macrocycle, it can be assumed that this intramolecular interaction is the trigger for the strong saddling deformation. In contrast, the other modes in the three systems behave very similar. The ruffling mode is

**Figure 8.** Linear displays of atomic dislocations from the mean-squares C<sub>20</sub>N<sub>4</sub> planes of **1**, **16**, and **14** (molecular structures from X ray diffraction studies).**Table 2.** NCD contributions of major distortion modes for **1**, **16**, and **14**.<sup>[16]</sup>

	saddling	ruffling	doming	wave (x + y)
<b>1</b> (Ph/py)	0.78	0.38	0.18	0.16
<b>16</b> (MeO/py)	0.99	0.30	0.09	0.29
<b>14</b> (F/dipy)	0.18	0.35	0.15	0.24

characterized, among other issues, by the adaptation of the macrocycle to the steric requirements of the central metal<sup>[17]</sup> – in this case zinc(II) – and shows medium size values. The weak doming mode depends largely on the type of central metal and the axial ligand. Significant differences between the pyrrolyl and dipyrrolyl derivatives are therefore not to be expected for these two modes.

The solution structures of the new isoporphyrins were investigated by means of NMR spectroscopy. As suggested by the results from X-ray diffraction, all pyrrolyl-substituted isoporphyrins studied turned out to exist as a single *syn* isomer with the pyrrolyl moiety and the axial chloro ligand situated at the same side of the macrocycle. These two subunits are connected via a N–H⋯Cl hydrogen bond as indicated by the low-field shift of the pyrrolic NH signal that is present in the <sup>1</sup>H NMR spectra between 10.37 ppm and 10.68 ppm for the zinc complexes, and at 9.92 ppm for the cadmium complex **11**. The spectra of zinc and cadmium *meso*-pyrrolyl isoporphyrins carrying benzene-related substituents all show 4 signals for the β-CH groups in the narrow range of 6.72 ppm to 6.32 ppm and thus outside the typical aromatic region. A minor shift of the individual signals generally follows the Hammett  $\sigma_p$  and  $\sigma_o$  constants<sup>[18]</sup> of the respective aryl groups (see Supporting Information). The NH and β-CH signals of the thienyl derivatives **8** and **9** are shifted to lower field by about 0.2–0.3 ppm. This may be related to the increased effective conjugation in these compounds, to their larger saddling mode amplitude, or both. For the less saddled dipyrrolyl derivatives **12–14** and **17**,<sup>[10]</sup> however, similar shifts of the β-CH signals are observed, so that an influence of the saddling mode on the <sup>1</sup>H NMR chemical shift is rather negligible.

The dipyrrolyl derivatives **12–14** show a double signal set of the same intensity in the <sup>1</sup>H- and <sup>13</sup>C NMR spectrum. This behavior was already described for **17** in the preliminary study<sup>[10]</sup> and could be attributed to the presence of two isomers by means of DOSY spectroscopy. In one isomer (*syn*), the dipyrrolyl unit points to the upper side of the macrocycle and is thus situated next to the chloro ligand, and in the other isomer (*anti*) to the lower side. The *anti* form is evident in the molecular structure of **14**. For NMR, however, the presence of two isomers in slightly different amounts and the often high

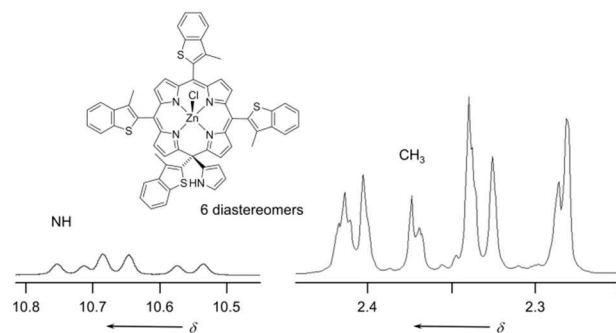


Figure 10. Details from the <sup>1</sup>H NMR spectrum of **10** (500 MHz, CD<sub>2</sub>Cl<sub>2</sub>).

number of partially broadened signals in the spectra makes it difficult to assign signals to the individual positions of the dipyrrolyl derivatives.

A particularly intriguing case comes with the methylbenzothienyl derivatives **10** and **15**. These compounds form as mixtures of several atropisomers due to the hindered rotation of the benzothienyl groups. As detailed in Figure 9, the pyrrolyl derivative **10** exists as a mixture of eight isomers in about equal ratio, including two pairs of enantiomers. This leads to six individual diastereomers, and thus to six overlapping NMR subspectra. These subspectra can in fact be observed for the NH resonances in the <sup>1</sup>H NMR spectrum (Figure 10). For the methyl group signals between 2.27 ppm and 2.42 ppm, symmetry predicts 20 individual lines in different ratios, of which only a fraction can be detected individually due to intense overlap. Even more complex are the spectra of the dipyrrolyl benzothienyl derivative **15** carrying yet another rotationally hindered benzothienyl substituent at the dipyrrolyl unit. Symmetry predicts 32 isomers (16 enantiomeric pairs) and thus 16 subspectra of similar intensities for this compound (see Supporting Information). Consequently, only groups of signals can be assigned in the <sup>1</sup>H NMR spectrum of **15**, and no meaningful <sup>13</sup>C NMR spectra were recorded. In general, there are even more possible isomers for the dipyrrolyl isoporphyrins **IV** as this moiety may reside not only in the geometry shown by the structural analysis of **14** but also with a rotated pyrrole ring, or with the positions of the aryl

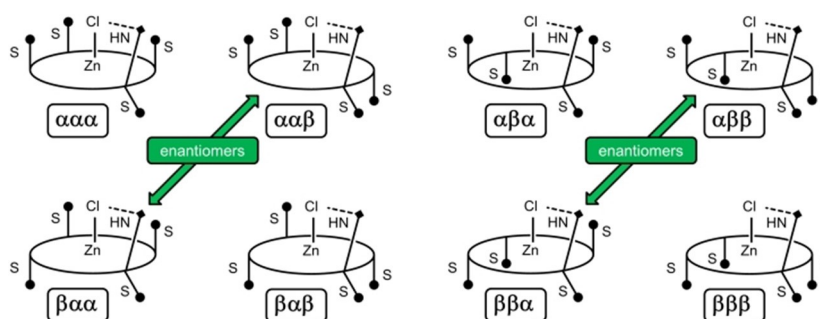


Figure 9. Schematic representation of the eight atropisomers of **10**, with indication of the pairs of enantiomers (ellipse: isoporphyrin perimeter in perspective view; S and full circle: orientation of the sulfur atom from the benzothienyl units; HN and full diamond: NH group from pyrrolyl unit). Only hydrogen bridge-stabilized *syn* forms are taken into consideration.

group and the pyrrole ring swapped, or both. These additional sets of isomers were, however, not taken into consideration as the NMR spectra of the compounds **12–14** and **17** only show two sets of signals, each for one *syn*- and one *anti* form.

The optical spectra of the new isoporphyrin derivatives with pyrrolyl and dipyrrolyl substitution are similar in habitus and band intensities to those of the systems already described, and differ only in details. An exception are again the thienyl derivatives, where particularly red-shifted absorptions are observed (Figure 11). The highest values are obtained for the methylbenzothienyl derivative **10** with  $\lambda_{\text{max}}=923$  nm. This special behavior of the thienyl derivatives is also observed for the dipyrrolyl isoporphyrins, where the most red-shifted absorption of the methylbenzothienyl derivative extends to 896 nm into the NIR range.

TD-DFT calculations were performed to support the optical properties of the isoporphyrins **1** and **8** on the CAM-B3LYP level of theory with the def-2/TZVP basis set in dichloromethane, using the conductor-like polarizable model (CPCM). The transitions with their composition and assignment are shown in Table S1. The long-wavelength transitions are mainly described by the HOMO→LUMO configuration for both macrocycles, while the more intense Soret-like bands at 350 nm to 470 nm correlate with several transitions between admixed states with contributions from HOMO, HOMO-2 and HOMO-6 on one side, and LUMO as well as LUMO+1 on the other. Within the usual margin of error for TD-DFT,<sup>[19]</sup> the calculated absorptions fit well with the experimental spectra and predict the observed red-shift for the Q band of thienyl isoporphyrin **8** (Figure 11).

As a final and hitherto inaccessible task, the redox behavior of isoporphyrins was investigated. Isoporphyrin and phlorin<sup>[20]</sup> are formally connected to each other by a  $2\text{H}^+ - 2\text{e}^-$  redox context, although this could not be experimentally proven so far due to the high sensitivity of isoporphyrins. To confirm this relationship, the electron transfer characteristics of zinc isoporphyrin **16** in acetonitrile were investigated using cyclic voltammetry (CV) and square wave voltammetry (SWV). As a result it could be shown that upon applying positive potentials only irreversible processes occur, in which the decomposition of

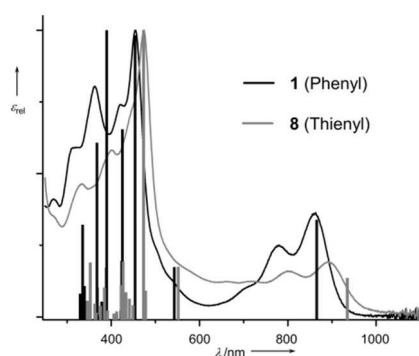


**Figure 11.** UV/Vis spectra ( $\text{CH}_2\text{Cl}_2$ ) of zinc isoporphyrins **1** and **8**, and results from TD-DFT calculations (bar plots). To visualize the assignment of the bands, the theoretical absorptions were shifted on the energy scale to fit the Soret-type band of the experimental spectra ( $3615\text{ cm}^{-1}$  for **1** and  $4155\text{ cm}^{-1}$  for **8**).

the electrooxidized species proceeds rapidly. At negative potentials, on the other hand, two waves can be detected during reduction and three waves during reoxidation (Figure 12). The signal at  $E_{1/2}=-950$  mV proves to be quasi-reversible at sufficiently high sweep rates, while the waves at  $E_{1/2}=-680$  mV and at  $E_{1/2}=-510$  mV are more susceptible to a change in the sweep rate (see Supporting Information) and thus suggest a coupling of the quasi-reversible electron transfer with a reversible chemical reaction (EC process).

To confirm the assumption that the nature of the chemical reaction is the dissociation and reassociation of the chloro ligand in the sense of the reaction diagram in Figure 12, the chloro ligand of **16** was exchanged for perchlorate, and the cationic zinc isoporphyrin thus obtained was also measured under the same conditions. In fact, the wave at  $E_{1/2}=-680$  mV disappears completely in favor of a quasi-reversible wave at  $E_{1/2}=-510$  mV. However, due to the limited chemical stability of the electroreduced species, neither the determination of the ligand exchange rate at the isoporphyrin radical nor the spectroelectrochemical analysis of the two-electron reduced species was successful. The formation of a zinc phlorinate could thus only be made probable, but not definitively proven.

## Conclusion

The present study has shown that the template-controlled one-pot synthesis of zinc isoporphyrins can be applied to many aromatic aldehydes. The limitations lie with certain electron deficient and sterically hindered derivatives, as well as with most heterocyclic systems, for which isoporphyrin formation cannot, or only in traces, be shown. The formation is particularly advantageous for thienyl derivatives. The introduction of these potentially electroactive side chains opens an important door for future processing in the context of molecular materials. However, the transfer of template synthesis to other metal ions

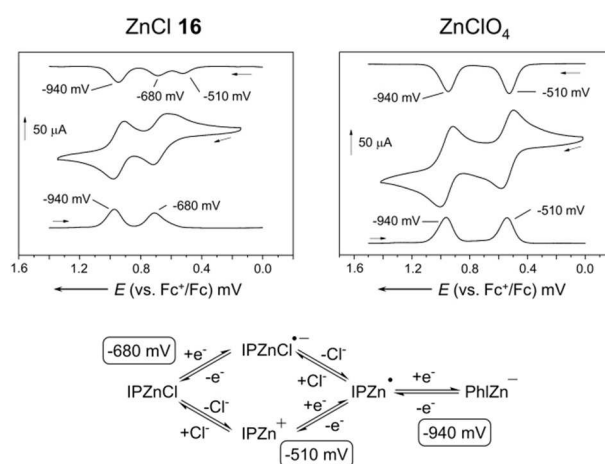


**Figure 12.** Assigned cyclic voltammograms and square wave voltammograms of **16** (left) and of the respective perchlorate (right; acetonitrile,  $0.4\text{ mol/L } n\text{-Bu}_4\text{NPF}_6$ , scanning speed  $1\text{ V/s}$ ), with proposed reaction scheme for **16** (IP = isoporphyrin; Phl = phlorin).

fails in almost all cases. Here, the further development of the demetallation-remetallation strategy starting from the zinc derivatives is necessary. This approach has already been shown to be viable in preliminary work<sup>[10]</sup> and is currently being further developed in our laboratories.

Aside of the synthetic aspects, important influences of the different substituents on structural and spectroscopic properties were also discovered. For example, the thienyl derivatives turn out to be particularly strongly saddled, which leads to red-shifted absorptions in the optical spectra and characteristic changes in the NMR spectra. The exclusive presence of an NH...Cl hydrogen bridge in the pyrrolyl derivatives **II** also forces the formation of a single atropisomeric form, provided that the aryl substituents do not exhibit significant rotational hindrance. The development of these derivatives in particular, which in two cases could already be optimized by the solvent composition during synthesis, thus holds great advantages.

Finally, first electrochemical studies on the redox behavior of zinc isoporphyrins could successfully be carried out, whereby two electroreduced forms proved to be sufficiently stable for qualitatively meaningful cyclic voltammograms. We are currently active in this area as well and looking forward to future results.

## Experimental Section

**General remarks:** Solvents were dried according to standard procedures and saturated with nitrogen. All reagents were purchased from commercial sources and used as received. CHN analyses were performed on an *Elementar Vario MicroCube* instrument. <sup>1</sup>H-, <sup>13</sup>C- and <sup>19</sup>F-NMR spectra were obtained on a *Bruker Avance II 300*, a *Bruker Avance III HD 500* and a *Bruker Avance II 600* spectrometer at room temperature. Chemical shifts ( $\delta$ ) are given in ppm relative to TMS and referenced against residual protio solvent resonances. Mass spectra were recorded on a *Thermo Scientific LXQ* instrument with electrospray source in positive mode. *m/z* values are given for the most abundant isotopes only. HRMS data was obtained using a *Thermo Finnigan MAT95 XL Trap* Instrument. UV-Vis data was collected in dichloromethane solution ( $c \sim 10^{-5}$  mol/L) on a *Varian Cary 50 Scan* spectrophotometer. Cyclic voltammetry and square wave voltammetry were performed with a *Princeton Applied Research VersaSTAT 3* potentiostat under inert conditions at room temperature in absolute acetonitrile containing 0.4 M *n*Bu<sub>4</sub>NPF<sub>6</sub>. A self-made 3-electrode set-up with two platinum wires as working and counter electrodes and a silver wire as quasi-reference electrode was used. The formal potentials  $E_{1/2}$  are given in mV relative to the ferrocenium/ferrocene couple. X-ray intensity data were collected at 100(2) K using a *Rigaku XtaLAB Synergy S Single Source* diffractometer (CuK $\alpha$ ). Each single crystal was mounted in inert perfluoroether oil on top of a glass fibre. Both structures were solved and refined using SHELXS-2014/7.<sup>[21]</sup> WinGX was used to prepare publication material.<sup>[22]</sup> Graphics were prepared using Mercury.<sup>[23]</sup>

**DFT and TD-DFT calculations for isoporphyrins 1 and 8:** For isoporphyrins chlorozinc-tetraphenyl-pyrrolylisoporphyrin **1** and chlorozinc-tetrathienylpyrrolyl-isoporphyrin **8** a geometry optimization with subsequent normal mode analysis was performed, starting from a structure based on geometric data obtained from X-ray diffraction analysis of the methoxy derivative **16**.<sup>[10]</sup> For all calculations ORCA in Version 4.1.1 has been used.<sup>[24]</sup> Geometry optimization was performed using GGA functional BP86<sup>[25]</sup> with

triple zeta def2-TZVP basis<sup>[26]</sup> using D3BJ dispersion correction.<sup>[27]</sup> Further optimization was performed using CAM-B3LYP hybrid exchange correlation functional<sup>[28]</sup> using the CPCM solvation model for dichloromethane with the same basis set. The obtained structure was then used for time-dependent density functional theory (TD-DFT) analysis requesting 20 states with disabled Tamm-Dancoff Approximation (TDA). The relevant orbitals have been exported as cube file which were then visualized using ChemCraft.<sup>[29]</sup>

### General procedure for the synthesis of zinc isoporphyrins 1–15:

Two 500 mL round bottom flasks each with 200 mL methanol and the respective aryl aldehyde (5 mmol) were treated with freshly distilled pyrrole (0.7 mL, 10 mmol) and HCl<sub>aq</sub> (36%, 5 mL) in water (200 mL). Both flasks were vigorously stirred at room temperature for 3 h, whereupon a solid residue formed. The mixtures were extracted with chloroform (3 × 100 mL), the organic layers combined, washed water (3 × 100 mL) and dried over Na<sub>2</sub>SO<sub>4</sub>. This solution was treated with metal acetate dihydrate (6.4 mmol) and to reflux. *p*-Chloranil (2.46 g, 10 mmol) is added to the hot mixture, and reflux is continued for 1 h. The solvent was removed under reduced pressure and the residue subjected to column chromatography on silica. CH<sub>2</sub>Cl<sub>2</sub> was used to wash the corrole byproduct **III** and some metal porphyrin off the silica, followed by CH<sub>2</sub>Cl<sub>2</sub>/ethyl acetate 10:1 to elute isoporphyrins **II** and, if present, **IV**. If necessary, repeated chromatography on silica with CH<sub>2</sub>Cl<sub>2</sub>/ethyl acetate mixtures (25:1 to 100:7) yielded pure pyrrolyl- and dipyrinyl isoporphyrins, which could be obtained as pure solids after recrystallisation from CH<sub>2</sub>Cl<sub>2</sub>/*n*-hexane. For the spectroscopic and analytical data of 1–15 see the Supporting Information.

**Crystallographic data :** Deposition numbers 2064672 (for **1**) and 2064673 (for **14**) contain the supplementary crystallographic data for this paper. These data are provided free of charge by the joint Cambridge Crystallographic Data Centre and Fachinformationszentrum Karlsruhe Access Structures service [www.ccdc.cam.ac.uk/structures](http://www.ccdc.cam.ac.uk/structures).

**Crystal data for 1:** C<sub>48</sub>H<sub>32</sub>ClN<sub>5</sub>Zn × CH<sub>2</sub>Cl<sub>2</sub>, *M* = 864.53, monoclinic, space group *P*<sub>2</sub><sub>1</sub>/*c*, *a* = 15.006(4) Å, *b* = 12.7874(4) Å, *c* = 20.4224(8) Å,  $\beta$  = 91.805(4)°, *V* = 3917(1) Å<sup>3</sup>, *Z* = 4,  $\rho_{\text{calc}}$  = 1.466 g cm<sup>-3</sup>,  $\mu(\text{Cu-K}\alpha)$  = 3.095 mm<sup>-1</sup>, *R*<sub>1</sub> [*I* > 2 $\sigma$ (*I*)] = 0.0645, *wR*<sub>2</sub> (all data) = 0.1876.

**Crystal data for 14:** C<sub>59</sub>H<sub>34</sub>ClF<sub>5</sub>N<sub>6</sub>Zn × CH<sub>2</sub>Cl<sub>2</sub>, *M* = 1092.25, monoclinic, space group *P*<sub>2</sub><sub>1</sub>/*n*, *a* = 11.3235(1) Å, *b* = 25.7658(3) Å, *c* = 18.2797(2) Å,  $\beta$  = 106.393(1)°, *V* = 5116.5(1) Å<sup>3</sup>, *Z* = 4,  $\rho_{\text{calc}}$  = 1.418 g cm<sup>-3</sup>,  $\mu(\text{Cu-K}\alpha)$  = 2.457 mm<sup>-1</sup>, *R*<sub>1</sub> [*I* > 2 $\sigma$ (*I*)] = 0.0526, *wR*<sub>2</sub> (all data) = 0.1584.

## Acknowledgements

This work was kindly funded by the Deutsche Forschungsgemeinschaft DFG, grant BR2010/15-1. The authors wish to express their gratitude to Niels Klein, Dr. Vitali Kuhn, Julian Oelmann, and Dr. Jörn Rösner for their help with mass spectrometry. Open access funding enabled and organized by Projekt DEAL.

## Conflict of Interest

The authors declare no conflict of interest.



**Keywords:** Conformation · isoporphyrin · one-pot synthesis · template synthesis · zinc

- [1] R. B. Woodward, *Pure Appl. Chem.* **1961**, *2*, 383–404.
- [2] D. Dolphin, R. H. Felton, D. C. Borg, J. Fajer, *J. Am. Chem. Soc.* **1970**, *92*, 743–745.
- [3] a) J. A. Guzinski, R. H. Felton, *J. Chem. Soc. Chem. Commun.* **1973**, 715–716; b) H. J. Shine, A. G. Padilla, S.-M. Wu, *J. Org. Chem.* **1979**, *44*, 4069–4075; c) K. M. Kadish, R. K. Rhodes, *Inorg. Chem.* **1981**, *20*, 2961–2966; d) A. Harriman, G. Porter, P. Walters, *J. Chem. Soc. Faraday Trans. 1* **1983**, *79*, 1335–1350; e) A. Gold, W. Ivey, G. E. Toney, R. Sangaiah, *Inorg. Chem.* **1984**, *23*, 2932–2935; f) E. S. Schmidt, T. C. Bruce, R. S. Brown, C. L. Wilkins, *Inorg. Chem.* **1986**, *25*, 4799–4800; g) W. A. Lee, T. C. Bruce, *Inorg. Chem.* **1986**, *25*, 131–135; h) M.-C. Richoux, P. Neta, P. A. Christensen, A. Harriman, *J. Chem. Soc. Faraday Trans. 2* **1986**, *82*, 235–249; i) A. Hinman, B. J. Pavelich, A. E. Kondo, S. Pons, *J. Electroanal. Chem. Interfacial Electrochem.* **1987**, *234*, 145–162; j) W. Szulbicki, J. W. Strojek, *J. Electroanal. Chem. Interfacial Electrochem.* **1988**, *252*, 323–334; k) Y. Takeda, S. Takahara, Y. Kobayashi, H. Misawa, H. Sakuragi, K. Tokumaru, *Chem. Lett.* **1990**, 2103–2106; l) S. Mosseri, J. C. Mialocq, B. Perly, P. Hambright, *J. Phys. Chem.* **1991**, *95*, 2196–2203; m) R. Guillard, N. Jagerovic, A. Tabard, C. Naillon, K. M. Kadish, *J. Chem. Soc. Dalton Trans.* **1992**, 1957–1966; n) H. Segawa, R. Azumi, T. Shimidzu, *J. Am. Chem. Soc.* **1992**, *114*, 7564–7565; o) S. Gentemann, S. H. Leung, K. M. Smith, J. Fajer, D. Holten, *J. Phys. Chem.* **1995**, *99*, 4330–4334; p) G. J. Abhilash, J. Bhuyan, P. Singh, S. Maji, K. Pal, S. Sarkar, *Inorg. Chem.* **2009**, *48*, 1790–1792; q) J. Bhuyan, S. Sarkar, *Chem. Eur. J.* **2010**, *16*, 10649–10652; r) Z. Cong, T. Kurahashi, H. Fujii, *J. Am. Chem. Soc.* **2012**, *134*, 4469–4472; s) J. Bhuyan, *Dalton Trans.* **2016**, *45*, 2694–2699; t) Y. J. Franzke, D. Sundholm, F. Weigend, *Phys. Chem. Chem. Phys.* **2017**, *19*, 12794–12803; u) K. D. Borah, J. Bhuyan, *J. Mol. Struct.* **2019**, *72*, 2251–2260.
- [4] R. Gericke, L. M. Doyle, E. R. Farquhar, A. R. McDonald, *Inorg. Chem.* **2020**, *59*, 13952–13961.
- [5] a) I. Garcia-Bosch, S. K. Sharma, K. D. Karlin, *J. Am. Chem. Soc.* **2013**, *135*, 16248–16251; b) M. A. Ehudin, L. Senft, A. Franke, I. Ivanović-Burmazović, K. D. Karlin, *J. Am. Chem. Soc.* **2019**, *141*, 10632–10643.
- [6] M. Boudiaf, Y. Liang, R. Lamare, J. Weiss, H. Ibrahim, M. Goldmann, E. Bentouhami, V. Badets, S. Choua, N. Le Breton, A. Bonnefont, L. Ruhlmann, *Electrochim. Acta* **2019**, *309*, 432–449.
- [7] a) H.-J. Kim, J. S. Lindsey, *J. Org. Chem.* **2005**, *70*, 5475–5486; b) J.-I. Setsune, A. Tsukajima, J. Watanabe, *Tetrahedron Lett.* **2006**, *47*, 1817–1820; c) G. Pomarico, X. Xiao, S. Nardis, R. Paolesse, F. R. Fronczek, K. M. Smith, Y. Fang, Z. Ou, K. M. Kadish, *Inorg. Chem.* **2010**, *49*, 5766–5774; d) D. L. Flint, R. L. Fowler, T. D. LeSaulnier, A. C. Long, A. Y. O'Brien, G. R. Geier, *J. Org. Chem.* **2010**, *75*, 553–563; e) J. Wojaczyński, M. Duszak, L. Latos-Grażyński, *Tetrahedron* **2013**, *69*, 10445–10449; f) C. M. Lemon, M. Huynh, A. G. Maher, B. L. Anderson, E. D. Bloch, D. C. Powers, D. G. Nocera, *Angew. Chem. Int. Ed.* **2016**, *55*, 2176–2180; *Angew. Chem.* **2016**, *128*, 2216–2180; g) M. Hoffmann, B. Cordes, C. Kleeberg, P. Schweyen, B. Wolfram, M. Bröring, *Eur. J. Inorg. Chem.* **2016**, 3076–3085; h) R. Wicht, S. Bahnmüller, K. Brandhorst, P. Schweyen, M. Bröring, *Chem. Sci.* **2016**, *7*, 583–588; i) R. Wicht, S. Bahnmüller, A. Thüsing, B. Wolfram, M. Bröring, *Eur. J. Inorg. Chem.* **2019**, 4477–4485.
- [8] J. Bhuyan, *Dalton Trans.* **2015**, *44*, 15742–15756.
- [9] a) H. Xie, K. M. Smith, *Tetrahedron Lett.* **1992**, *33*, 1197–1200; b) K. M. Barkigia, M. W. Renner, H. Xie, K. M. Smith, J. Fajer, *J. Am. Chem. Soc.* **1993**, *115*, 7894–7895; c) H. Xie, S. H. Leung, K. M. Smith, *J. Porphyrins Phthalocyanines* **2002**, *6*, 607–616; d) S. C. Mwakwari, H. Wang, T. J. Jensen, M. G. H. Vicente, K. M. Smith, *J. Porphyrins Phthalocyanines* **2011**, *15*, 918–929.
- [10] P. Schweyen, M. Hoffmann, J. Krumsieck, B. Wolfram, X. Xie, M. Bröring, *Angew. Chem. Int. Ed.* **2016**, *55*, 10118–10121; *Angew. Chem.* **2016**, *128*, 10272–10275.
- [11] a) A. D. Adler, F. R. Longo, J. D. Finarelli, J. Goldmacher, J. Assour, L. Korsakoff, *J. Org. Chem.* **1967**, *32*, 476; b) A. Ghosh, *Angew. Chem. Int. Ed.* **2004**, *43*, 1918–1931; *Angew. Chem.* **2004**, *116*, 1952–1931.
- [12] B. Koszarna, D. T. Gryko, *J. Org. Chem.* **2006**, *71*, 3707–3717.
- [13] L. Simkhovich, I. Goldberg, Z. Gross, *Org. Lett.* **2003**, *5*, 1241–1244.
- [14] M. O. Senge, S. A. MacGowan, J. M. O'Brien, *Chem. Commun.* **2015**, *51*, 17031–17063.
- [15] For zinc complexes of linear oligopyrroles, see: a) Y. Murakami, Y. Matsuda, Y. Kanaoka, *Bull. Chem. Soc. Jpn.* **1971**, *44*, 409–415; b) D. W. Hutchinson, B. Johnson, A. J. Knell, *Biochem. J.* **1973**, *133*, 399–400; c) G. Struckmeier, U. Thewalt, J.-H. Fuhrhop, *J. Am. Chem. Soc.* **1976**, *98*, 278–279; d) W. S. Sheldrick, J. Engel, *J. Chem. Soc. Chem. Commun.* **1980**, 5–6; e) R. Bonnett, D. G. Buckley, D. Hamzetaş, *J. Chem. Soc. Perkin Trans. 1* **1981**, 322–325; f) M. Bröring, S. Link, C. D. Brandt, E. Cónsul Tejero, *Eur. J. Inorg. Chem.* **2007**, 1661–1670.
- [16] a) W. Jentzen, X. Z. Song, J. A. Shelnutt, *J. Phys. Chem. B* **1997**, *101*, 1684–1699; b) C. J. Kingsbury, M. O. Senge, *Coord. Chem. Rev.* **2021**, *431*, 213760.
- [17] a) J. Rösner, B. Cordes, S. Bahnmüller, G. Homolya, D. Sakow, P. Schweyen, R. Wicht, M. Bröring, *Angew. Chem. Int. Ed.* **2017**, *56*, 9967–9970; *Angew. Chem.* **2017**, *129*, 10099–9970; b) P. Schweyen, C. Kleeberg, D. Körner, A. Thüsing, R. Wicht, M.-K. Zaretske, M. Bröring, *J. Porphyrins Phthalocyanines* **2020**, *24*, 303–313.
- [18] C. Hansch, A. Leo, R. W. Taft, *Chem. Rev.* **1991**, *91*, 165–195.
- [19] S. Dreuw, M. Head-Gordon, *Chem. Rev.* **2005**, *105*, 4009–4037.
- [20] a) B. Krattinger, H. J. Callot, *Eur. J. Org. Chem.* **1999**, 1857–1867; b) J.-W. Ka, C.-H. Lee, *Tetrahedron Lett.* **2001**, *42*, 4527–4529; c) D. T. Gryko, B. Koszarna, *Eur. J. Org. Chem.* **2005**, 3314–3318; d) D. Kim, H.-J. Chun, C. C. Donnelly, G. R. Geier III, *J. Org. Chem.* **2016**, *81*, 5021–5031.
- [21] G. M. Sheldrick, *Acta Crystallogr. Sect. A* **2008**, *64*, 112–122.
- [22] L. J. Farrugia, *J. Appl. Crystallogr.* **2012**, *45*, 849–854.
- [23] C. F. Macrae, I. J. Bruno, J. A. Chisholm, P. R. Edgington, P. McCabe, E. Pidcock, L. Rodriguez-Monge, R. Taylor, J. van de Streek, P. A. Wood, *J. Appl. Crystallogr.* **2008**, *41*, 466–470.
- [24] a) F. Neese, *WIREs Comput. Mol. Sci.* **2012**, *2*, 73–78; b) F. Neese, *WIREs Comput. Mol. Sci.* **2018**, *8*, e1327.
- [25] a) J. P. Perdew, K. Burke, M. Ernzerhof, *Phys. Rev. Lett.* **1996**, *77*, 3865–3868; b) A. D. Becke, *Phys. Rev. A* **1988**, *38*, 3098–3100.
- [26] a) F. Weigend, *Phys. Chem. Chem. Phys.* **2006**, *8*, 1057–1065; b) F. Weigend, R. Ahlrichs, *Phys. Chem. Chem. Phys.* **2005**, *7*, 3297–3305.
- [27] a) S. Grimme, J. Anthony, S. Ehrlich, H. Krieg, *J. Chem. Phys.* **2010**, *132*, 154104; b) S. Grimme, S. Ehrlich, L. Goerigk, *J. Comput. Chem.* **2011**, *32*, 1456–1465.
- [28] a) A. D. Becke, *J. Chem. Phys.* **1993**, *98*, 5648–5652; b) C. Lee, W. Yang, R. G. Parr, *Phys. Rev. B* **1988**, *37*, 785–789; c) P. J. Stephens, F. J. Devlin, C. F. Chabalowski, M. J. Frisch, *J. Phys. Chem.* **1994**, *98*, 11623–11627; d) S. H. Vosko, L. Wilk, M. Nusair, *Can. J. Phys.* **1980**, *58*, 1200–1211; e) T. Yanai, D. P. Tew, N. C. Handy, *Chem. Phys. Lett.* **2004**, *393*, 51–57; f) B. Miehlich, A. Savin, H. Stoll, H. Preuss, *Chem. Phys. Lett.* **1989**, *157*, 200–206.
- [29] *Chemcraft – Graphical software for visualization of quantum chemistry computations*, <https://www.chemcraftprog.com>.

Manuscript received: February 24, 2021

Accepted manuscript online: April 7, 2021

Version of record online: May 7, 2021